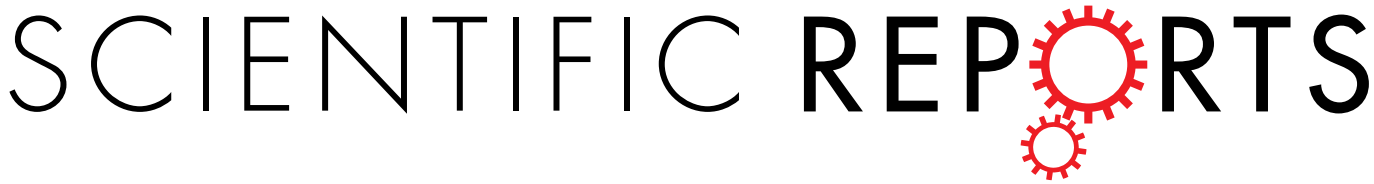

OPEN

Received: 24 June 2015
Accepted: 21 September 2015
Published: 19 October 2015

Electronic Structure and Ferromagnetism Modulation in Cu/Cu_2O Interface: Impact of Interfacial Cu Vacancy and Its Diffusion

Hao-Bo Li[1], Weichao Wang[1,4], Xinjian Xie[2], Yahui Cheng[1], Zhaofu Zhang[1], Hong Dong[1], Rongkun Zheng[3], Wei-Hua Wang[1], Feng Lu[1] & Hui Liu[1]

Cu/Cu_2O composite structures have been discovered to show sizable ferromagnetism (FM) with the potential applications in spintronic devices. To date, there is no consensus on the FM origin in Cu/Cu_2O systems. Here, first principles calculations are performed on the interface structure to explore the microscopic mechanism of the FM. It is found that only the Cu vacancy (V_{Cu}) adjacent to the outermost Cu_2O layer induces a considerable magnetic moment, mostly contributed by 2*p* orbitals of the nearest-neighbor oxygen atom (O_{NN}) with two dangling bonds and 3*d* orbitals of the Cu atoms bonding with the O_{NN}. Meanwhile, the charge transfer from Cu to Cu_2O creates higher density of states at the Fermi level and subsequently leads to the spontaneous FM. Furthermore, the FM could be modulated by the amount of interfacial V_{Cu}, governed by the interfacial Cu diffusion with a moderate energy barrier (~1.2 eV). These findings provide insights into the FM mechanism and tuning the FM via interfacial cation diffusion in the Cu/Cu_2O contact.

Diluted magnetic semiconductors (DMS) are promising materials for spintronic devices due to the employment of the spin degree of freedom besides the charge property of carriers[1,2]. Among the III-V semiconductors doped by transition metals, spin polarization of carriers is achieved in Mn-doped GaAs, InAs and etc[3,4]. However, the low Curie temperature far below room temperature impedes the DMS-based device development[5]. In recent years, oxides diluted magnetic semiconductors (ODMS), such as Fe-ZnO, Cr-TiO_2, Mn-TiO_2 and etc, have attracted much attention due to their Curie temperature over 300 K in regards to DMS[6–8]. Unexpectedly, room temperature ferromagnetism (FM) has been observed in undoped oxides. After Venkatesan and Coey *et al.* pioneered in the finding of the room-temperature FM in undoped HfO_2[9], other oxides without intentional magnetic impurities doping are subsequently discovered to show the FM behavior[10–12].

Significant investigations of the FM mechanism are performed on the undoped nanoscaled ODMS systems, such as fine powder, heterostructures, core-shell nanoparticles and etc, where the surface and interfacial native point defects are supposed to be the origin of the FM[13–16]. However, without the contribution of magnetic transition metal ions, the traditional magnetic exchange interactions in oxides,

[1]Department of Electronics and Tianjin Key Laboratory of Photo-Electronic Thin Film Device and Technology, Nankai University, Tianjin, 300071, China. [2]School of Materials Science and Engineering, Hebei University of Technology, Tianjin, 300130, China. [3]School of Physics, the University of Sydney, NSW, 2006, Australia. [4]Department of Materials Science and Engineering, The University of Texas at Dallas, Richardson, Texas 75080, United States. Correspondence and requests for materials should be addressed to W.-H.W. (email: whwangnk@nankai.edu.cn) or F.L. (email: lufeng@nankai.edu.cn)

including long range double-exchange or super-exchange, are no longer suitable for depicting the FM in these systems. Therefore, a charge transfer Stoner model is proposed to fundamentally understand the FM induced by defects[17–19]. The criterion of Stoner model requires $D(E_F)J > 1$, where $D(E_F)$ is the density of states at the Fermi level (E_F) and J denotes the strength of exchange interaction. Spontaneous FM is triggered when a large $D(E_F)$ occurs. Nevertheless, it is still not accessible how surface and interfacial defects introduce the localized states around Fermi level, and finally result in a large $D(E_F)$ through the charge transfer. It is thus critical to unveil the connection between the FM and the defects states.

Relative to *n*-type ODMS, the *p*-type ODMS are much less explored. As a natural *p*-type material, cuprous oxide (Cu_2O) is a promising material as catalyst, transistors, and etc[20,21]. If Cu_2O could possess room-temperature FM, Cu_2O would not only act as one spintronic material but also offer a fundamental platform to study the correlation between FM and structural properties. Actually, cuprous oxide (Cu_2O) has shown room-temperature FM as other undoped oxides[9–12]. To date, there is no consensus of the origin of the FM in undoped Cu_2O. Theoretically, the FM in undoped Cu_2O is claimed to be induced by the oxygen interstitial in the bulk and by unsaturated Cu in the surface[22]. Experimentally, the undoped Cu_2O fine powder[13], nanowires[23], and CuO/Cu_2O interface[24] all exhibit the room-temperature FM relevant with the cation defects. Especially in our previous experimental work in Cu/Cu_2O core-shell nanoparticles, the FM is found to be closely connected with the Cu vacancy (V_{Cu})[25]. Besides, the magnetization can be tuned by modulating the V_{Cu} amount through controlling the oxygen partial pressure and the annealing duration. Basically, it is critical to clarify the microscopic mechanism of V_{Cu} induced FM and the feasibility to tune the FM through V_{Cu} generation or compensation.

In this work, we have performed the density functional theory (DFT) calculations on the Cu/Cu_2O interface in order to elucidate the origin and the modulation of FM. Our results indicate that the defect-free Cu/Cu_2O interface is nonmagnetic, but in contrast, the interface containing specific site of V_{Cu} possesses FM. The FM is not directly contributed by the V_{Cu} but mostly contributed by the nearest-neighbor oxygen atom (O_{NN}) and the Cu atoms (Cu_{NN}) bonding with the O_{NN}. As the anti-bonding states between the O_{NN} and the Cu_{NN} form localized states near the valence band maximum (VBM), the E_F is pinned at the localized states and a large $D(E_F)$ is satisfied through the charge-transfer from Cu to Cu_2O at the interface. A moderate energy barrier (~1.2 eV) of the Cu diffusion guarantees the feasibility of modulating the FM through controlling the amount of interfacial V_{Cu}. Our results provide an insight to understand the origin and the modulation of the FM in Cu/Cu_2O contact.

Results and Discussion

Stabilities of Cu/Cu_2O interfaces with different interfacial Cu and O contents. The Cu(111) surface is the most stable in terms of the surface coordination[26]. When the Cu(111) surface is oxidized, an intrinsic Cu(111)/Cu_2O(111) interface forms[27,28]. In this work, we focus on the Cu(111)/Cu_2O(111) intrinsic interface, labeled as Cu/Cu_2O. The bulk and surface calculations ensure that five layers slab model is suitable for the further interface exploration (See Supplementary Information).

Five sandwich-like layers of Cu_2O(111) surface and five layers of Cu(111) surface are included in a slab model with a 15 Å vaccum space, where the top Layer 1 (see Supplementary Information Figure S1) of the Cu_2O(111) contacts with the Cu(111) and the bottom Layer 5 is passivated. In practice, oxide surface reconstruction plays an important role to influence the interface quality. Thus, in order to capture this important structural information, we consider Cu_2O surface reconstruction here. As a recent scanning tunneling microscopy (STM) result proposed, under different oxidation conditions, $\sqrt{73}R5.8° \times \sqrt{21}R10.9°$ structure (also known as the "44" surface) is one of the stable Cu_2O(111) surface reconstructions[26]. Therefore, in this work, we concentrate on the interface Cu/Cu_2O based on this specific "44" surface reconstruction. Referring to Soon *et al.*[29], we constructed the Cu/Cu_2O interface by a 2×2 Cu(111) surface and a 4×4 Cu_2O(111) surface. Due to the better ductibility of the metal Cu than semiconductor Cu_2O, the lattice parameters of Cu_2O are kept constant in Cu/Cu_2O interface structures. The lattice mismatch for Cu is ~2.7%. According to the interfacial copper and oxygen contents, several candidate interface structures are considered. Figure 1(a,b) are top and side views of the pristine Cu/Cu_2O interface (int-pristine). Figure 1(c,d) present two and one Cu_{uns} atoms in the Cu_2O part, respectively (int-2Cu_{uns}, int-1Cu_{uns}). Figure 1(e,f) are top and side views of the interface without Cu_{uns} atoms in the Cu_2O part (int-zero-Cu_{uns}). Figure 1(g,j) are interfaces with additional adsorbed oxygen atoms based on the int-zero-Cu_{uns}. According to the O_{ads} locations and amount, they are labeled as int-1O_{ads}-A, int-1O_{ads}-B and int-2O_{ads}, respectively.

To determine the most stable interface, the interface free (formation) energy is calculated using the following equation,

$$\gamma = \left(E_{interface} - N_{Cu}\mu_{Cu}^{bulk} - N_{Cu_2O}\mu_{Cu_2O} \pm l_O\mu_O\right)/A \quad (1)$$

where $E_{interface}$ is the interface total energy. N_{Cu} and N_{Cu_2O} denote the amount of Cu atom and Cu_2O primitive unit, respectively. μ_{Cu}^{bulk}, and μ_O are the chemical potentials of bulk Cu, and oxygen in bulk Cu_2O. Here, μ_{Cu_2O} represents the energy of one Cu_2O primitive cell. l_O is the number of the excess or deficient oxygen atoms in the interface. A is the interface area. The chemical potentials $\mu_{Cu}^{Cu_2O}$ and μ_O in Cu_2O possess the relationship of:

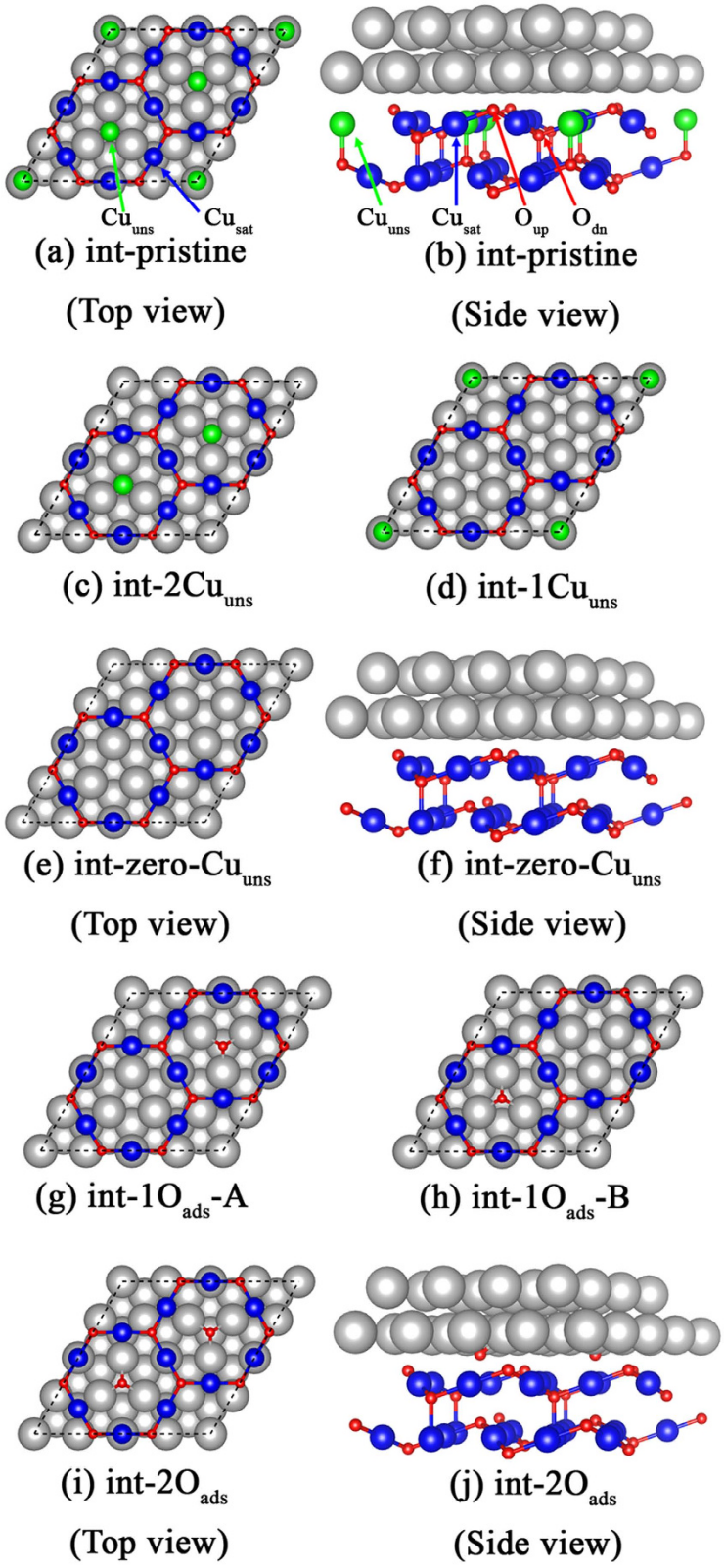

Figure 1. Top and side views of Cu/Cu2O interface with pristine structure, int-pristine in (**a**) and (**b**). Part of the interfacial Cu_{uns} atoms present, two and one Cu_{uns} in (**c**) int-2Cu_{uns} and (**d**) int-1Cu_{uns}). Top and side views of interface without interfacial $Cu_{uns,}$ int-zero-Cu_{uns} in (**e**,**f**). Interfaces with additional adsorbed oxygen atoms based on the int-zero-Cu_{uns}. According to the O_{ads} locations and amount, they are labeled as int-1O_{ads}-A in (**g**), int-1O_{ads}-B in (**h**) and int-2O_{ads} in (**i**,**j**). Large silver balls are Cu atoms in Cu(111) surface. Green and blue balls denote the Cu_{uns} and Cu_{sat} in Cu_2O, respectively. Small red balls are oxygen atoms.

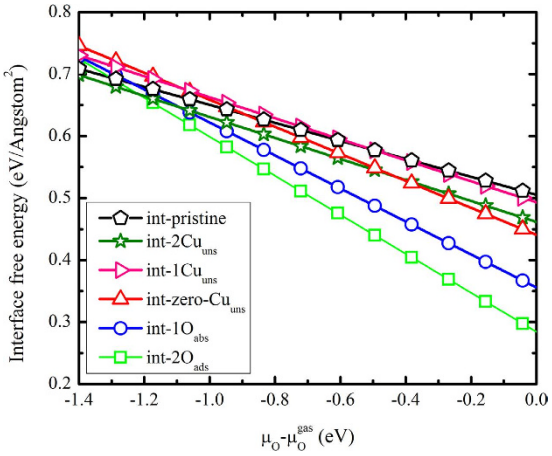

Figure 2. Dependence of interface free (formantion) energy for different structures on the oxygen chemical potential. The int-2O_{ads} structure is found to be the most stable interface structure.

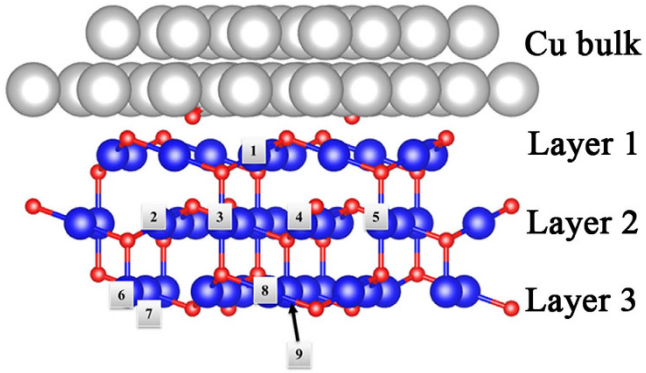

Figure 3. The numbers from 1 to 9 demonstrate the possible V_{Cu} locations in Cu/Cu_2O int-2Oads interface after introducing one V_{Cu}.

$$2\mu_{Cu}^{Cu_2O} + \mu_O = \mu_{Cu_2O} \tag{2}$$

where $\mu_{Cu}^{Cu_2O}$ is the chemical potential of Cu in Cu_2O.

As we know, the maximum of chemical potential for one element occurs in its elemental phase. Combined with formula (2), μ_O is restricted in following range:

$$\mu_{Cu_2O} - 2\mu_{Cu}^{bulk} \leq \mu_O \leq \mu_O^{gas} \tag{3}$$

which can be rewritten as:

$$\Delta H_{Cu_2O}^f \leq \mu_O - \mu_O^{gas} \leq 0 \tag{4}$$

The calculated $\Delta H_{Cu_2O}^f$ is −1.24 eV (See Supplementary Information Table S1), which is consistent with generalized gradient approximation (GGA) result[29]. The μ_O^{gas}, half of an oxygen molecule energy, is −4.92 eV. The interface formation energies of different interfaces are plotted in Fig. 2. All structures tend to become more stable as μ_O increases. The int-2O_{ads} structure possesses the lowest interface energy when $\mu_O - \mu_O^{gas}$ is in the range of −1.2 to 0.0 eV, which agrees with the reference work[29].

Microscopic mechanism of the ferromagnetism induced by Cu vacancy. Since the Cu vacancies are closely correlated with the interface FM[25], one V_{Cu} is introduced into in the most stable int-2O_{ads} interface. The possible V_{Cu} locations are labeled as int-2O_{ads}-V_{Cu}(n) in Fig. 3, where n denotes the location number. Following the definition of Cu atom in the Cu_2O surface (see Supplementary Information Figure S1), two types of Cu vacancy (Cu_{uns} and Cu_{sat}) are called as "uns" and "sat" in Table 1. Through

Structure	Type of V_{Cu}	V_{Cu} location	Charge transfer from Cu to Cu_2O (e)	Total magnetic moment (μ_B)
int-$2O_{ads}$	N/A	N/A	2.58	0.000
int-$2O_{ads}$-V_{Cu}(1)	sat	Layer 1	2.79	0.000
int-$2O_{ads}$-V_{Cu}(2)	sat	Layer 2	2.57	0.501
int-$2O_{ads}$-V_{Cu}(3)	uns		2.60	0.000
int-$2O_{ads}$-V_{Cu}(4)	sat		2.57	0.420
int-$2O_{ads}$-V_{Cu}(5)	uns		2.62	0.000
int-$2O_{ads}$-V_{Cu}(6)	uns	Layer 3	2.58	0.002
int-$2O_{ads}$-V_{Cu}(7)	sat		2.58	0.000
int-$2O_{ads}$-V_{Cu}(8)	sat		2.58	0.001
int-$2O_{ads}$-V_{Cu}(9)	uns		2.58	0.000

Table 1. Total magnetic moment and the amount of charge transfer from Cu to Cu_2O in int-$2O_{ads}$ with one V_{Cu} at different locations.

the collinear spin-polarized calculations, the charge transfer from Cu to Cu_2O is characterized based on the Bader charge analysis (Table 1)[30], from which we find that Cu_2O gains ~2.6 electrons. Such charge transfer originates from the different work functions (WF) between Cu (WF: 4.6 eV) and Cu_2O (WF: 4.8 eV)[31,32]. Among the int-$2O_{ads}$-V_{Cu}(n) systems, int-$2O_{ads}$-V_{Cu}(1) exhibits the largest charge transfer (~2.8 e) owing to the new bond formation between the Cu_2O and the Cu surface.

According to Table 1, it is noticed that not all kinds of V_{Cu} introduce a large magnetic moment into the interface system. Only vacancy at Cu_{sat} in Layer 2 contributes a relatively large magnetic moment (0.4 to 0.5 μ_B) among all these structures. In order to unveil the FM mechanism, the interface band structures of defect-free int-$2O_{ads}$ and int-$2O_{ads}$-V_{Cu}(2) are calculated in Fig. 4(a,b). The green lines represent the total band structure of the interface. The dots and the triangles indicate the contribution from Layer 2 (see Supporting Information Figure S1) where the V_{Cu}(2) locates, and the size denotes the weight. Compared with the bulk contribution, more localized surface states are observed near the E_F, and the spin-up and spin-down states are splitted, indicating the Stoner instability. The existence of each V_{Cu} leaves two dangling bonds with respect to its two nearest-neighbor oxygen atoms (O_{NN}). These dangling bonds may play a key role to introduce the FM. For more direct visual confirmation, the spin resolved projected density of states (PDOS) of O_{NN} 2p and the 3d orbitals of the Cu atom (Cu_{NN}) bonding with the O_{NN} are plotted in Fig. 4(c). Around the E_F, the O_{NN}-2p spin-up anti-bonding states (−1 to 0 eV) are mostly occupied and the spin-down anti-bonding states are partially occupied. Meanwhile, due to the anti-bonding states composed by O_{NN}-2p and Cu_{NN}-3d orbitals, the Cu_{NN}-3d orbitals show spin splitting as well. To compare the local magnetic moment within the same range, the spin-density distribution of int-$2O_{ads}$-V_{Cu}(2) is visualized within an atom sphere radius 0.8 Å which accords to the Wigner Seitz radius of oxygen atom (Fig. 4(d)). It demonstrates that the upper O_{NN} contributes a relatively large proportion of magnetic moment (0.138 μ_B), while each Cu_{NN} produces 0.075 μ_B. Even when the radius is increased to 1.0 Å, the local magnetic moment on O_{NN} and Cu_{NN} are 0.147 μ_B and 0.08 μ_B, respectively, which is quite similar to the above results. In a word, in terms of the FM origin, the magnetic moment at the Cu/Cu_2O interface is mainly from O_{NN} and the Cu_{NN} atoms. The magnetic moment on Cu_{NN} results from the spin-splitting 3d orbitals which forms anti-bonding states with O_{NN}-2p orbitals.

To further illustrate the origin of the FM contributed by the O_{NN}, the PDOS of the O_{NN}-2p and Cu_{NN}-3d orbitals in different locations of V_{Cu} are presented in Fig. 5. Referring to Fig. 3, the PDOS for two types of V_{Cu} locations, one "uns" and one "sat" in each layer, are provided here. Each V_{Cu} has two O_{NN} atoms, and for clarity, only the PDOS of O_{NN} with more dangling bonds are shown here. In the bulk Cu_2O, the O_{NN}-2p and Cu_{NN}-3d orbitals generate large localized defect states in the range from −5.0 eV to −4.0 eV below the VBM. Meanwhile, a delocalized band near the VBM is also created. The state around the E_F indicates that the hole produced by V_{Cu} and occupies a valence band like perturbed-host state (PHS)[33]. Comparing with the bulk Cu_2O, the O_{NN}-2p and Cu_{NN}-3d orbitals also create localized bonding states from −5.0 eV to −4.0 eV below the E_F and delocalized states around the E_F when V_{Cu} is not at site 2. However, besides the deep localized states in int-$2O_{ads}$-V_{Cu}(2) moving up to the range from −4.0 eV to −3.0 eV, the prominently localized states appear around the E_F. In other words, the Femi level could be pinned by these localized states. To understand this pinning phenomenon, we calculate the energy difference (ΔE) between the E_F and the VBM of Cu_2O. For the defect-free int-$2O_{ads}$ interface, this energy difference is 0.12 eV. However in the int-$2O_{ads}$-V_{Cu}(2) interface, ΔE is also ~0.12 eV. Since the localized defect states induced by the V_{Cu}(2) would pin the E_F at the certain location and the charge transfer would not obviously shift E_F, the FM occurs consequently.

To investigate why only certain V_{Cu} could create localized states around the E_F, we focus on the dangling bonds character of the O_{NN}. Generally, the O atoms in Cu_2O bulk form four bonds with the nearest

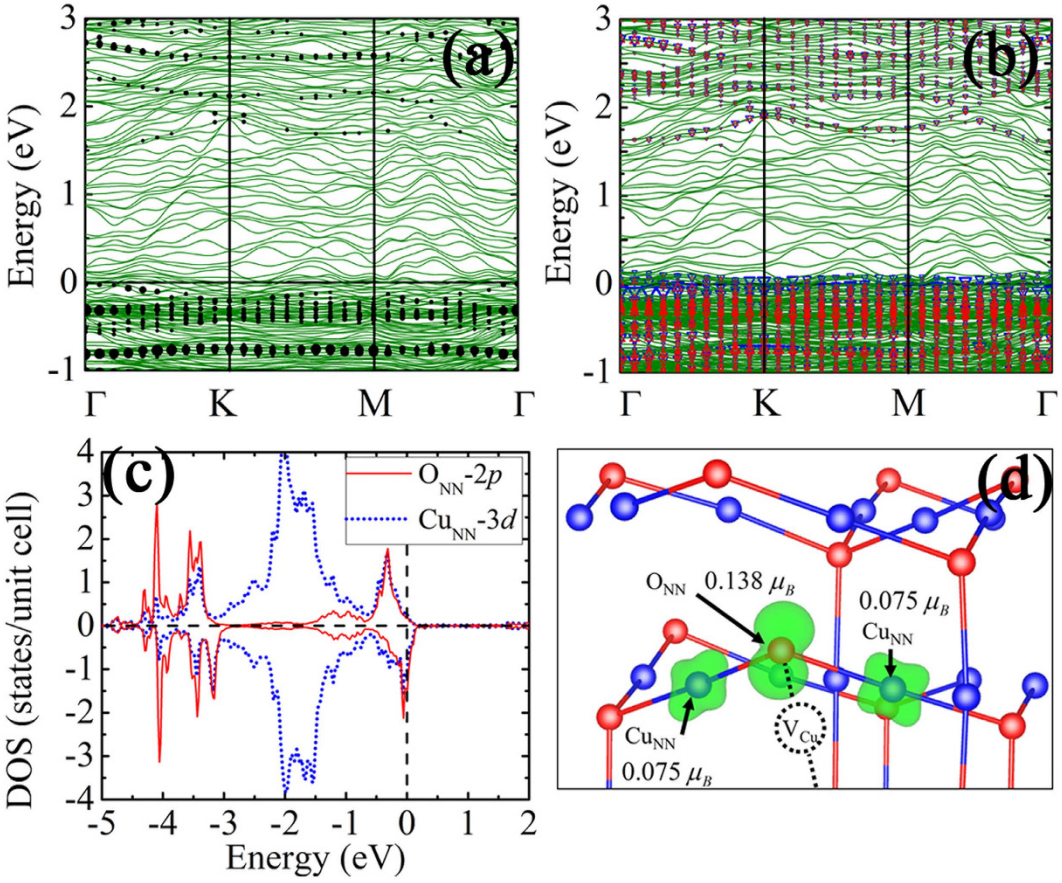

Figure 4. (**a**) The spin-restricted band structure of defect-free int-pristine interface, and the dots from the contribution by Cu_2O-Layer 2. (**b**) The spin-polarized band structure of int-$2O_{ads}$-V_{Cu}(2). The up (down) triangles represent the spin-up (down) states of Cu_2O-Layer 2. (**c**) The projected DOS of the O_{NN} and Cu_{NN} in int-$2O_{ads}$-V_{Cu}(2) interface. (**d**) The spin-densities of the O_{NN} and Cu_{NN} and the corresponding magnetic moments within the atom sphere of radius 0.8 Å.

four Cu atoms. Hence one O_{NN} around the V_{Cu} forms bonds with three other Cu atoms, generating one dangling bond. The spin-polarized calculation for a $2 \times 2 \times 2$ bulk Cu_2O supercell with one Cu vacancy gives the magnetic moment per atom less than $0.0001\,\mu_B$, indicating a non-magnetic state. However, in the int-$2O_{ads}$-V_{Cu}(2) interface, the upper O_{NN} is merely bonding with two Cu atoms due to the natural "uns"-V_{Cu} presence in Layer 1 (Fig. 5(b)). Therefore, the unique int-$2O_{ads}$-V_{Cu}(2) interface structure provides O_{NN} one more dangling bonds, which leads to the weaker *p-d* hybridization and a more localized O-2*p* wave functions. For int-$2O_{ads}$-V_{Cu}(1), a new bond between the O_{NN} and the Cu atom in above Cu(111) surface in the relaxed structure, as shown in Fig. 5(c). The new bond length is 1.95 Å, which is shorter than that in other int-$2O_{ads}$-V_{Cu}(n) structures (~2.07 Å). Thus, the new bond formation leads to the delocalized O_{NN}-2*p* orbitals and the quenching of spin magnetic moment. It implies that once the dangling bonds are compensated, the larger magnetic moment shrinks.

Modulation of the ferromagnetism driven by interfacial Cu diffusion. The FM in Cu/Cu_2O interface is sensitive to the annealing process, in which the amount of the V_{Cu} responsible for the FM could be tunable. It is important to investigate the feasibility of the Cu diffusion through the interface. Actually, the Cu diffusion from Cu into Cu_2O is observed in previous experiments[34,35]. Such diffusion may degrade the electrical performance in Cu_2O thin-film transistors[36] and modulate the magnetism during the Cu oxidation. Up to date, the theoretical Cu diffusion process and the energy barrier (E_b) in Cu/Cu_2O contact are not well understood. Hence, a thoroughly study on the energy barrier related to the Cu diffusion and its influence on the FM is performed by climb image nudge elastic band (CI-NEB) calculations. As the int-$2O_{ads}$-V_{Cu}(2) structure has the largest magnetic moment, we focus on the Cu diffusion in this structure. As the V_{Cu} in int-$2O_{ads}$-V_{Cu}(2) structure is located in Layer 2 (see Fig. 3), the diffusion process could be divided into two steps as shown in Fig. 6(a). The first step is one Cu atom moving from the Cu(111) surface into the natural V_{Cu} located in Layer 1, leaving a vacancy on Cu(111) surface behind. Following the first step, this specific Cu atom further diffuses into V_{Cu}(2) in Layer 2 (see Fig. 3). Once the V_{Cu} in Layer 2 is compensated, the FM almost vanishes. Within the CI-NEB calculations, the

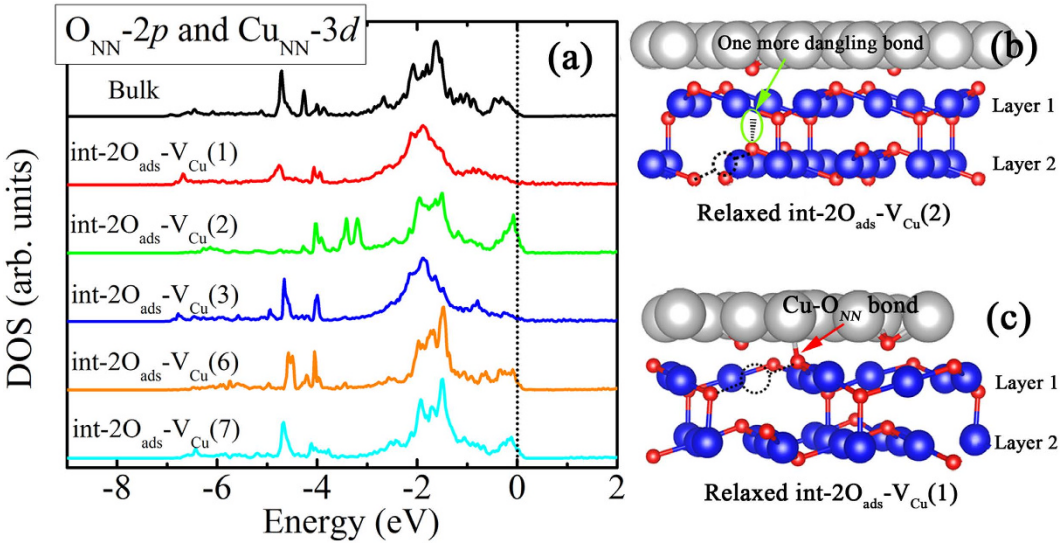

Figure 5. (**a**) The PDOS of O_{NN}-2*p* and corresponding Cu_{NN}-3*d* orbitals in int-2O_{ads}-V_{Cu}(n) interface. For clarity, the PDOS for two types of V_{Cu} structures, "uns" and one "sat" in each layer in Fig. 5, and the O_{NN} with the more dangling bonds are presented. (**b**) The relaxed int-2O_{ads}-V_{Cu}(2) interface structure. Two dangling bonds of O_{NN} are observed due to the natural presence of "uns" type V_{Cu} in Layer 1. (**c**) The relaxed int-2O_{ads}-V_{Cu}(1) structure. The O_{NN} actually forms a new bond with one Cu atom from upper Cu surface, resulting only one dangling bond of O_{NN}. The dotted circles represent the location of V_{Cu}.

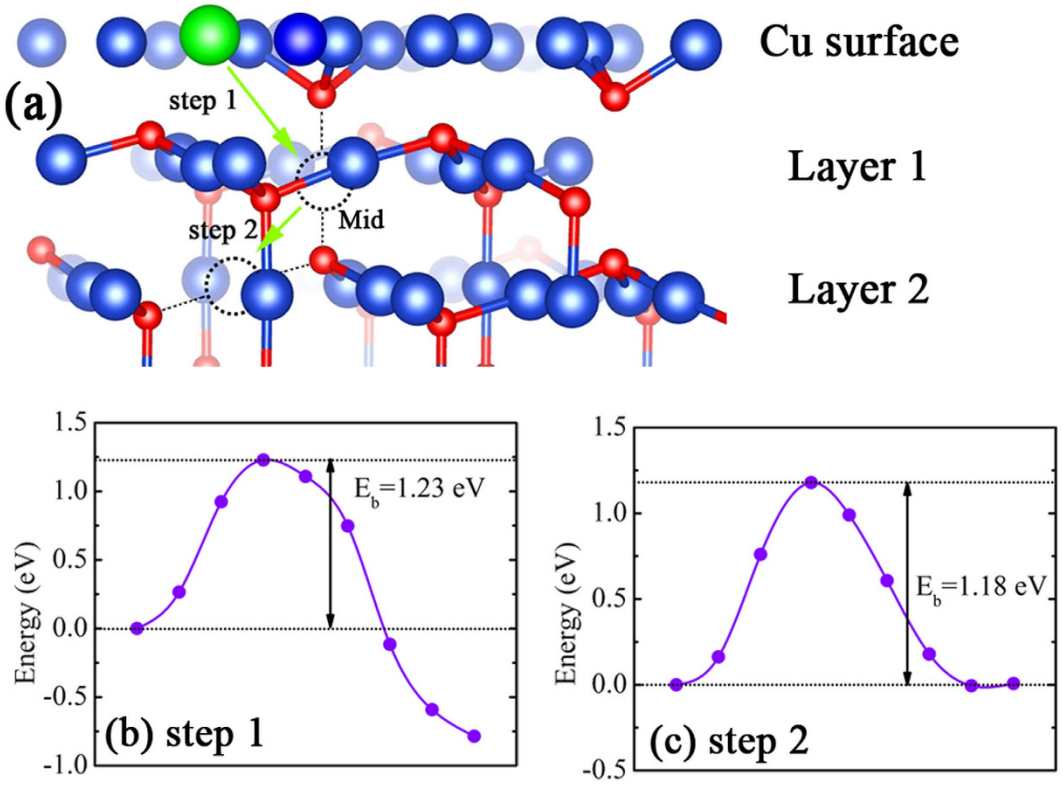

Figure 6. (**a**) Cu diffusion route from Cu(111) surface to the V_{Cu} site in int-2O_{ads}-V_{Cu}(2) structure. The energy curves in (**b**,**c**) corresponding to the first and the second step during the diffusion. The dotted circles represent the different reaction coordinates in NEB calculations.

energy barrier (E_b) is found to be 1.23 eV in the first step, and the total energy drops by 0.79 eV in the final stage, as plotted in Fig. 6(b). Such energy barrier is ~0.2 eV higher than the activation energy (E_a) in the Cu_2O growth by oxidation (~1.0 eV)[37,38]. The Cu_2O growth from Cu oxidation is closely related with the Cu diffusion from Cu to Cu_2O[39]:

$$(1 + \alpha) D_{\mathrm{Cu}} = k_p \tag{5}$$

where α and D_{Cu} are the degree of ionization of defects and diffusion coefficient of Cu, respectively. k_p denotes the parabolic rate which could be obtained by:

$$k_p = k_p^0 p_{O_2}^{1/4} e^{-E_a/(kT)} \tag{6}$$

where k_p^0 is a prefactor and p_{O_2} represents the partial pressure in oxidation. Actually, the activation energy (E_a) is the energy barrier (E_b) in the Cu oxidation process, which determines the Cu diffusion. Please refer to the link "http://en.wikipedia.org/wiki/Activation_energy" for the definition of activation energy. According to the Arrhenius formula, the relationship between D_{Cu} and the diffusion energy barrier (E_b) can be written in the following equation:

$$D_{\mathrm{Cu}} = \lambda \nu d^2 e^{-E_b/(kT)} \tag{7}$$

Thus,

$$\lambda \nu d^2 e^{-E_b/(kT)} \propto k_p^0 p_{O_2}^{1/4} e^{-E_b/(kT)} \tag{8}$$

in which λ is a dimensionless factor, ν and d indicate the vibration frequency (normally $10^{12} \sim 10^{13}\,s^{-1}$) and the jump distance, respectively. When $p_{O_2} = 0.0015\mathrm{Torr}$ (0.2 Pa)[25], $k_p^0 p_{O_2}^{1/4} = 6.3 \times 10^{-5} cm^2 s^{-1}$ ($k_p^0 = 3.19 \times 10^{-4} cm^2 s^{-1} Torr^{-1/4}$ in ref. 40), d should be several angstroms to make D_{Cu} compatible for both sides of Eq. (8), which demonstrates that the Cu diffusion (~4 Å in the first step and ~3 Å in the second step) could be achievable. In Fig. 6(c), the E_b in the second step is 1.18 eV which is slightly less than that in the first step. The lower E_b in the second step implies that the Cu further moves easily to the V_{Cu} in the second layer of $Cu_2O(111)$ as well once it reaches the Cu_2O surface.

At the middle location (labeled as "Mid" in Fig. 6) in the whole diffusion process, the spin-polarized calculation is performed. The total magnetic moment, only 0.0003 μ_B, indicates that the diffused Cu suppresses the FM. At the "Mid" site, the diffused Cu forms bonds with the O_{NN} and the local magnetic moment drops significantly because partial dangling bonds of O_{NN} are compensated. A higher $D(E_F)$ of the Stoner criterion is no longer satisfied, which leads to the quenching of the FM. Thus during the growth of Cu_2O under Cu oxidation, the annealing treatment would influence the Cu diffusion. To further quantify the diffusion feasibility, the approximated diffusion time can be solved by[39]:

$$L = \sqrt{2 k_p t} \tag{9}$$

where L denotes the obtained oxidized layer (Cu_2O) thickness after the oxidization duration of t. When $E_b = 1.2$ eV and oxygen partial pressure is 0.2 Pa, the first step diffusion (~4 Å) would be finished in *about 40 minutes*. This result explains the experimental observation[25]. Therefore, the FM modulated by the annealing process in experiment is actually realized by controlling the amount of interfacial V_{Cu} through Cu diffusion within the Cu/Cu_2O interface.

Conclusion

To summarize, the FM in Cu/Cu_2O contact is induced by V_{Cu} around the Cu/Cu_2O interface. Only the interface structure with the "sat" type V_{Cu} in the second layer possesses a relatively large magnetic moment due to two dangling bonds of O_{NN}. The E_F is pinned in the O_{NN}-2p and Cu_{NN}-3d localized states and a large $D(E_F)$ is achieved by the charge transfer from Cu to Cu_2O. Once the V_{Cu} is compensated by the diffused Cu atom, the number of dangling bonds reduces and the FM vanishes. A moderate energy barrier (~1.2 eV) guarantees the feasibility to modulate the FM by controlling Cu diffusion in experiment. These results offer a comprehensive understanding about the microscopic mechanism of the FM and its modulation by V_{Cu} in Cu/Cu_2O interface. Also, our calculations provide an insight to understand and tune the FM relevant with defects in other metal/oxides contacts.

Calculation methods

All the calculations are performed using Vienna *ab initio* simulation package (VASP). The generalized gradient approximation (GGA) with exchange-correlation function of Perdew-Burke -Ernzerhof (PBE) is chosen[40]. The energy cutoff of 400 eV is selected and the electronic optimization stops when the total energies of neighboring optimization loops differ below 10^{-5} eV in all the calculations. A $7 \times 7 \times 7$ Monkhorst-Pack k-point mesh is set up in the bulk calculations. To avoid the interaction between periodic images, the vacuum thickness is set up to 15 Å for the surface and interface slab structures. The

Γ-centered $5 \times 5 \times 1$ *k*-point mesh is adopted in slab calculations. For the structural relaxation, the force on each atom is chosen to be less than 0.001 eV/Å in bulk calculations and less than 0.05 eV/Å in surface and interface calculations. The Cu diffusion paths are calculated by the climb image nudge elastic band (CI-NEB) method[41].

References

1. Wolf, S. A. *et al.* Spintronics: A spin-based electronics vision for the future. *Science* **294,** 1488–1495 (2001).
2. Matsumoto, Y. Room-temperature ferromagnetism in transparent transition metal-doped titanium dioxide *Science* **291,** 854–856 (2001).
3. Rüster, C. *et al.* Very large magnetoresistance in lateral ferromagnetic (Ga,Mn)As wires with nanoconstrictions. *Phys. Rev. Lett.* **91,** 216602 (2003).
4. Ohno, H. *et al.* Electric-field control of ferromagnetism. *Nature* **408,** 944–946 (2000).
5. Chen, L. *et al.* Enhancing the Curie temperature of ferromagnetic semiconductor (Ga,Mn)As to 200 K via nanostructure engineering. *Nano Lett.* **11,** 2584–2589 (2011).
6. Han, S. J. *et al.* A key to room-temperature ferromagnetism in Fe-doped ZnO: Cu. *Appl. Phys. Lett.* **81,** 4212 (2002).
7. Zhang, X. *et al.* Effect of oxygen partial pressure on the ferromagnetism of Cr-doped TiO_2 films *J. Phys. D: Appl. Phys.* **41,** 015005 (2008).
8. Mi, W. B., Liu, Y. W., Jiang, E. Y. & Bai, H. L. High-temperature ferromagnetism observed in facing-target reactive sputtered $Mn_xTi_{1-x}O_2$ films *Acta Mater.* **56,** 3511–3515 (2008).
9. Venkatesan, M., Fitzgerald, C. B. & Coey, J. M. D. Thin films: Unexpected magnetism in a dielectric oxide. *Nature* **430,** 630 (2004).
10. Pemmaraju, C. D. & Sanvito, S. Ferromagnetsim driven by intrinsic point defects in HfO_2. *Phys. Rev. Lett.* **94,** 217205 (2005).
11. Liu, H. *et al.* Role of point defects in room-temperature ferromagnetism of Cr-doped ZnO. *Appl. Phys. Lett.* **91,** 072511 (2007).
12. Peng, H. W. *et al.* Origin and enhancement of hole-induced ferromagnetism in first-row d^0 semiconductors. *Phys. Rev. Lett.* **102,** 017201 (2009).
13. Chen, C. P. *et al.* Magnetic properties of undoped Cu_2O fine powders with magnetic impurities and/or cation vacancies. *J. Phys.: Condense Matter* **21,** 145601 (2009).
14. Gao, D. Q. *et al.* Abnormal room temperature ferromagnetism in CuO-ZnO heterostructures: Interface related or not? *Chem. Commun.* **51,** 1151–1153 (2015).
15. Li, L. Y. *et al.* Room-temperature ferromagnetism and the scaling relation between magnetization and average granule size in nanocrystalline Zn/ZnO core–shell structures prepared by sputtering. *Nanotechnology* **21,** 145705 (2010).
16. Kapilashrami, M., Xu, J., Ström, V., Rao, K. V. & Belova, L. M. Transition from ferromagnetism to diamagnetism in undoped ZnO thin films. *Appl. Phys. Lett.* **95,** 033104 (2009).
17. Coey, J. M. D. & Chambers, S. A. Oxide dilute magnetic semiconductors—fact or fiction? *MRS Bulletin* **33,** 1054–1058 (2008).
18. Coey, J. M. D., Wongsaprom, K., Alaria, J. & Venkatesan, M. Charge-transfer ferromagnetism in oxide nanoparticles. *J. Phys. D: Appl. Phys.* **41,** 134012 (2008).
19. Chen, S. J., Suzuki, K. & Garitaonandia, J. S. Room temperature ferromagnetism in nanostructured ZnO-Al system. *Appl. Phys. Lett.* **95,** 172507 (2009).
20. Ai, Z. H., Zhang, L. Z., Lee, S. C. & Ho, W. Interfacial hydrothermal synthesis of $Cu@Cu_2O$ core-shell microspheres with enhanced visible-light-driven photocatalytic activity. *J. Phys. Chem. C* **113,** 20896 (2009).
21. Zou, X. A. *et al.* Top-gate low-threshold voltage *p*-Cu_2O thin-film transistor grown on SiO_2/Si substrate using a high-κ HfON gate dielectric. *IEEE Electron Device Lett.* **31,** 827–829 (2010).
22. Soon, A., Cui, X. Y., Delley, B., Wei, S. H. & Stampfl, C. Native defect-induced multifarious magnetism in nonstoichiometric cuprous oxide: First-principles study of bulk and surface properties of $Cu_{2-\delta}O$. *Phys. Rev. B* **79,** 035205 (2009).
23. Liao, L. *et al.* P-type electrical, photoconductive, and anomalous ferromagnetic properties of Cu_2O nanowires. *Appl. Phys. Lett.* **94,** 113106 (2009).
24. Gao, D. Q., Zhang, Z. P., Yang, Z. L. & Xue, D. S. Interface mediated ferromagnetism in bulk CuO/Cu_2O composite. *Appl. Phys. Lett.* **101,** 132416 (2012).
25. Li, H. B. *et al.* Room-temperature ferromagnetism in nanocrystalline Cu/Cu2O core-shell structures prepared by magnetron sputtering. *APL Mat.* **1,** 042106 (2013).
26. Matsumoto, T. *et al.* Scanning tunneling microscopy studies of oxygen adsorption on Cu(111). *Surf. Sci.* **471,** 225–245 (2001).
27. Dubois, L. H. Oxygen chemisorption and cuprous oxide formation on Cu(111): A high resolution EELS study. *Surf. Sci.* **119,** 399–410 (1982).
28. Pierson, J. F., Wiederkehr, D. & Billard, A. Reactive magnetron sputtering of copper, silver, and gold. *Thin Solid Films* **478,** 196–205 (2005).
29. Soon, A., Todorova, M., Delley, B. & Stampfl, C. Oxygen adsorption and stability of surface oxides on Cu(111): A first-principles investigation. *Phys. Rev. B* **73,** 165424 (2006).
30. Henkelman, G., Arnaldsson, A. & Jónsson, H. A fast and robust algorithm for Bader decomposition of charge density. *Comput. Mater. Sci.* **36,** 254–360 (2006).
31. Michaelson, H. B. The work function of the elements and its periodicity. *J. Appl. Phys.* **48,** 4729–4733 (1977).
32. Olsen, L. C., Bohara, R. C. & Urie, M. W. Explanation for low-efficiency Cu_2O Schottky-barrier solar cells. *Appl. Phys. Lett.* **34,** 47–49 (1979).
33. Raebiger, H., Lany, S. & Zunger, A. Origins of the p-type nature and cation deficiency in Cu_2O and related materials. *Phys. Rev. B* **76,** 045209 (2007).
34. Tylecote, R. F. The Composition and Reduction of Oxide Films on Copper. *Metallurgia* **53,** 191–197 (1956).
35. Zhu, Y., Mimura, K. & Isshiki, M. The effect of impurities on the formation of the inner porous layer in the Cu_2O scale during copper oxidation. *Oxidation of Metals* **61,** 293–301 (2004).
36. Fortunato, E., Barquinha, P. & Martins, R. Oxide semiconductor thin-film transistors: A review of recent advances. *Adv. Mater.* **24,** 2945–2986 (2012).
37. Matsumura, H., Fujii, A. & Kitatani, T. Properties of high-mobility Cu_2O films prepared by thermal oxidation of Cu at low temperatures. *Jpn. J. Appl. Phys.* **35,** 5631–5636 (1996).
38. Zhu, Y., Mimura, K. & Isshiki, M. Purity Effect on Oxidation Kinetics of Copper at 800–1050 °C. *J. Electrochem. Soc.* **151,** B27–B32 (2004).
39. Biccari, F. Defects and Doping in Cu_2O, *PhD Thesis, Sapienza, Univ. of Rome*, December, (2009).
40. Perdew, J. P., Burke, K. & Ernzerhof, M. Generalized gradient approximation made simple. *Phys. Rev. Lett.* **77,** 3865–3868 (1996).
41. Henkelman, G., Uberuaga, B. P. & Jónsson, H. J. A climbing image nudged elastic band method for finding saddle points and minimum energy paths. *J. Chem. Phys.* **113,** 9901–9904 (2000).

Acknowledgements

This work was supported by the NSF of China (Nos 11104148, 51171082, 11304161 and 11404172), 1000 youth talents plan, Tianjin NSF (Nos 13JCYBJC41100, 14JCZDJC37700 and 13JCQNJC02800), the National Basic Research Program of China (973 Program with No 2014CB931703), the SRFDP (20110031110034), and Fundamental Research Funds for the Central Universities. Parts of the calculations were performed at the Texas Advanced Computing Center (TACC) in Austin (http://www.tacc.utexas.edu).

Author Contributions

W.-H.W., F.L. and W.W. proposed the research idea. H.-B.L. performed the calculation. All the authors in the author-list devoted to the discussions and wrote the manuscript.

Additional Information

Supplementary information accompanies this paper at http://www.nature.com/srep

Competing financial interests: The authors declare no competing financial interests.

How to cite this article: Li, H.-B. *et al.* Electronic Structure and Ferromagnetism Modulation in Cu/Cu_2O Interface: Impact of Interfacial Cu Vacancy and Its Diffusion. *Sci. Rep.* **5**, 15191; doi: 10.1038/srep15191 (2015).